

# Coupling leeside grainfall to avalanche characteristics in aeolian dune dynamics

Joanna M. Nield<sup>1\*</sup>, Giles F.S. Wiggs<sup>2</sup>, Matthew C. Baddock<sup>3</sup>, and Martin H.T. Hipondoka<sup>4</sup>

<sup>1</sup>Geography and Environment, University of Southampton, Southampton, SO17 1BJ, UK

<sup>2</sup>School of Geography and the Environment, University of Oxford, Oxford, OX13QY, UK

<sup>3</sup>Department of Geography, Loughborough University, Loughborough, LE113TU, UK

<sup>4</sup>Department of Geography, University of Namibia, Private Bag 13301, Windhoek, Namibia

## ABSTRACT

**Avalanche (grainflow) processes are fundamental drivers of dune morphodynamics and are typically initiated by grainfall accumulations. In sedimentary systems, however, the dynamism between grainfall and grainflow remains unspecified because simple measurements are hampered by the inherent instability of lee slopes. Here, for the first time, terrestrial laser scanning is used to quantify key aspects of the grainfall process on the lee (slip face) of a barchan sand dune. We determine grainfall zone extent and flux and show their variability under differing wind speeds. The increase in the downwind distance from the brink of peak grainfall under stronger winds provides a mechanism that explains the competence of large avalanches to descend the entire lee slope. These findings highlight important interactions between wind speed, grainfall, and subsequent grainflow that influence dune migration rates and are important for correct interpretation of dune stratigraphy.**

## INTRODUCTION

Avalanching or grainflow, where sediment accumulation from grainfall leads to exceedance of the repose angle and results in downslope transport by gravity, is a fundamental process in sedimentary bedform development. In aeolian environments, avalanching is the principal mechanism for dune dynamism, and the cross-strata that grainflows produce can provide a record of dune accumulation and formation. Broader insights taken from avalanche processes observed on subaerial dunes can also aid our understanding of bedforms in other geomorphic systems. For example, lee slope depositional processes are particularly problematic to measure in large fluvial systems where sediment transport is greatest close to the bed (Kostaschuk et al., 2009). In extraterrestrial environments, interpretations of Martian aeolian wind patterns and dune activity have been derived from photographic evidence of dune leeside processes (Silvestro et al., 2010), where such analyses can only be enhanced by improved Earth analogue detail. Furthermore, avalanche deposits are a significant component of preserved aeolian stratigraphy, thus an understanding of avalanche processes provides important information for interpreting the rock record (Eastwood et al., 2012; Hunter, 1977).

Understanding leeside deposition processes is crucial for quantifying dune behavior, but until recently the instability and dynamic nature of these slopes have confounded detailed measurements of active processes. Technological

advancements, particularly the development of terrestrial laser scanning (TLS), now permits nondisruptive, sequential, high-resolution topographic surveying of unstable avalanche slopes, and allows quantification of morphological change at the scale of individual avalanches. While insights have been gained into slope angle criticality and relaxation as well as sediment flux-avalanche frequency relationships both in laboratory (Sutton et al., 2013a, 2013b) and field settings (Pelletier et al., 2015), it is the dynamics of grainfall accumulation as a destabilizing process that ultimately triggers grainflow. Classic works have modeled (Anderson, 1988) and measured (Nickling et al., 2002) sediment fallout rates and their controls, but there have been no recent advances specifically relating to grainfall processes. This is despite such dynamics representing the connection between sand flux at the dune brink, leeside avalanching dynamics, and dune migration.

In this field-based study we employ new technology to make novel quantifications of the aeolian grainfall process and its relationship to avalanching. In doing so, we shed light on the fundamental drivers of leeside deposition on dunes and the geomorphological mechanisms that result in aeolian dune migration.

## STUDY SITE AND METHODS

The Huab Valley dunefield in the Skeleton Coast National Park of northwest Namibia consists of migratory barchan dunes responding to predominant south-southwest winds (Hesp and Hastings, 1998; Lancaster, 1982). The avalanche

dynamics on a lee slope of a migrating barchan were measured during periods of sand transport on 4 and 5 September 2014. The dune (13.487°E, 20.869°S) was 5.12 m high, 95 m long, 69.5 m wide, and had a slip face of 8 m horizontal length (Fig. 1).

The average wind speed was measured on the dune centerline 1.1 m upwind of the brink at an interval of 10 Hz using a Campbell CSAT3 three-dimensional sonic anemometer at 0.5 m height. Colocated saltation measurements (from which saltation flux,  $Q_{sz}$ , was calculated; Barchyn et al., 2014) were recorded at the same frequency using a Wenglor gate sensor at 0.02 m height.

Avalanche dynamics on the lee slope of the barchan were measured using a Leica P20 Scanstation TLS (resolution of 1.6 mm at 10 m), positioned 10 m downwind from the base of the lee slope along the dune centerline (Fig. 1). The TLS remained in place for the duration of the ~3 h observations on each day with errors estimated

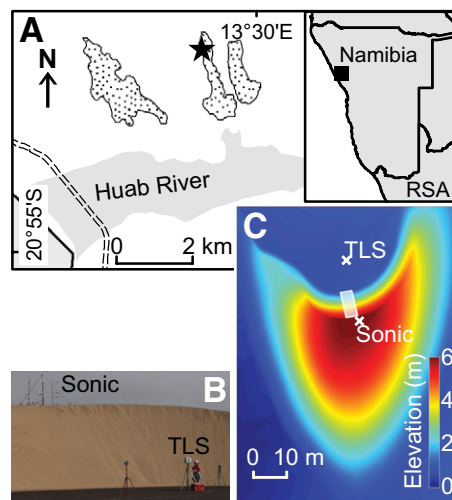


**Figure 1. A: Huab location within Namibia and map of study site; star indicates dune location. Stippled areas indicate areas of barchan and other aeolian deposits constituting the Huab dunefield. B: Lee slope experimental set-up. C: Digital elevation model of study barchan with placement of sonic anemometer and terrestrial laser scanner. The scanned area is indicated by the shaded rectangle.**

\*E-mail: J.Nield@soton.ac.uk

at 3 mm (Hodge et al., 2009). We focused on a 3.4-m-wide section of the lee slope adjacent to the brink instruments and dune centerline and perpendicular to the oncoming wind that took 46 s to scan. Measurements of the slope surface were repeated every 285 s. The TLS is able to detect saltating grains as partial signals above the slip face surface (Nield et al., 2011). This enables the quantification of the maximum length of travel of grains from the dune brink before being deposited on the lee slope as grainfall. Within each scan period, maximum grainfall length (i.e., the maximum horizontal downwind distance of grainfall above the lee slope) was determined as the maximum distance from the brink where one or more TLS point cloud measurements were detectable  $>0.025$  m above the slope surface (Nield and Wiggs, 2011). This enabled an indication of the 95<sup>th</sup> percentile of grainfall length ( $GL_{95}$ ) in 0.01 m across-slope bins for each period. The saltation flux ( $Q_{sz}$ ) over the brink was distributed by the 0.01 m binned grainfall frequency distribution to produce a horizontally distributed vertical grainfall flux ( $Q_g$ ) characterized by the grainfall flux mode ( $Q_{gm}$ ).

Lee slope topographic change was quantified by differencing TLS measurements gridded at 0.01 m. The deposition rate ( $\delta_D$ ) for each period was determined from surface elevation change in the top 1 m of the slip face, for the areas where avalanching had not occurred further downslope. This specification eliminated any influence of avalanche-caused topographic change, surmounting a significant methodological issue raised by Pelletier et al. (2015).

## RESULTS

Figure 2A shows strong positive exponential relationships between measured wind speed at the brink and both TLS-determined grainfall length ( $GL_{95}$ ) and maximum grainfall distributed flux ( $Q_{gm}$ ) with  $R^2$  values of 0.87 and 0.76, respectively. A strong nonlinear relationship is also seen between saltation flux at the brink ( $Q_{sz}$ ) and  $GL_{95}$  ( $R^2$  0.89; Fig. 2B). The plateauing of this curve reveals that at higher levels of  $Q_{sz}$  ( $>2$  kg m<sup>-2</sup> s<sup>-1</sup>), the  $GL_{95}$  does not increase downslope very rapidly, so that the increasing  $Q_{gm}$  becomes more concentrated on the upper lee slope (within 1 m of the brink) as  $Q_{sz}$  increases.

The  $\delta_D$  within the top 1 m of the lee slope also shows a strong positive and linear relationship with wind velocity ( $R^2$  0.79) (Fig. 3A), while the decay of  $\delta_D$  with distance from the brink is best represented by an exponential relationship (Fig. 3B). This measured decay in  $\delta_D$  is comparable to values of  $\delta_D$  decay measured directly using flux samplers (Hunter, 1985; McDonald and Anderson, 1995; Nickling et al., 2002; Sutton et al., 2013b). Figure 3B also highlights the influence of wind speed on the shape of the decay curve with the location of the maximum value of  $\delta_D$  shifting from 0.04 m to 0.06 m downwind of

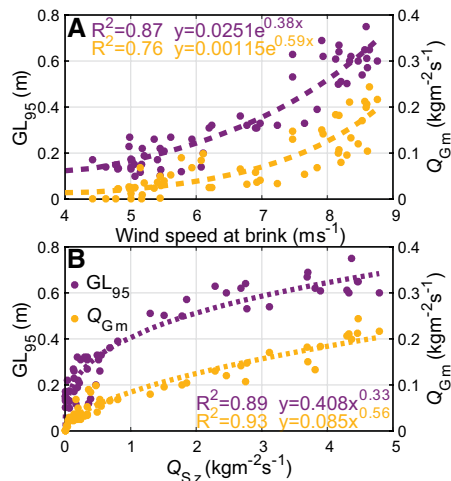
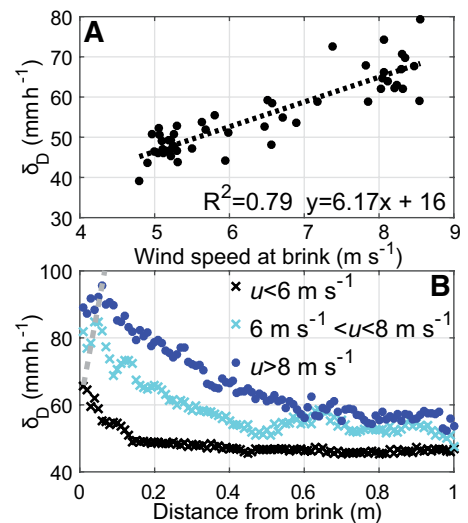


**Figure 2. A:** Wind speed measured at the brink, and, **B:** saltation flux ( $Q_{sz}$ ) to 95th percentile of measured grainfall length ( $GL_{95}$ ) and maximum value of the derived grainfall flux ( $Q_{gm}$ ) on the lee slope.

the brink as winds increase from  $<6$  m s<sup>-1</sup> to  $>8$  m s<sup>-1</sup>.

The influence of wind speed on the characteristics of  $GL_{95}$  and  $Q_{gm}$  is directly reflected in avalanche behavior. Figure 4A shows a surface change map of the lee slope between two scan periods during low wind ( $u = 5.2$  m s<sup>-1</sup>) with little saltation flux over the brink ( $Q_{sz} = 0.13$  kgm<sup>-2</sup> s<sup>-1</sup>). The calculated value of  $GL_{95}$  indicates that grainfall is focused within the top 0.21 m of the lee slope. Under such low wind speed (i.e.,  $u < 6$  m s<sup>-1</sup>), avalanche activity is typically characterized by the occurrence of small, discrete failures occurring close to the brink, with narrow necks ( $<0.34$  m) and limited deposition lobe length ( $<2.14$  m) and thickness ( $<0.018$  m). Such avalanches produce small erosion zones ( $<0.59$  m length) that are characteristic of the minimum accumulation that is capable of initiating avalanching. As mean wind speed,  $Q_{gm}$ , and  $GL_{95}$  increase, failures initiate further down the lee slope and larger avalanches become capable of reaching the bottom of the slip face (Fig. 4B;  $u = 6.5$  m s<sup>-1</sup>;  $GL_{95} = 0.32$  m). Under strong winds ( $u = 8.4$  m s<sup>-1</sup>), avalanches occur as multiple families of failures, with primary avalanches at the top and secondary failures partway down the slope, resulting in the frequent descent of grainflows over the entire slope to the slip face base (Fig. 4C).  $GL_{95}$  in Figure 4C is 0.67 m and the erosion zone at the top of the slip face expands under these higher wind conditions. Maximum widths and lengths of eroded areas increased to 0.77 m and 1.92 m, respectively, for winds  $>6$  m s<sup>-1</sup>. Likewise, the deposition lobes also increased in length and thickness under these stronger winds (4.7 m and 0.03 m, respectively).

The downslope extent of failure of the lee slope in changing wind conditions is shown in



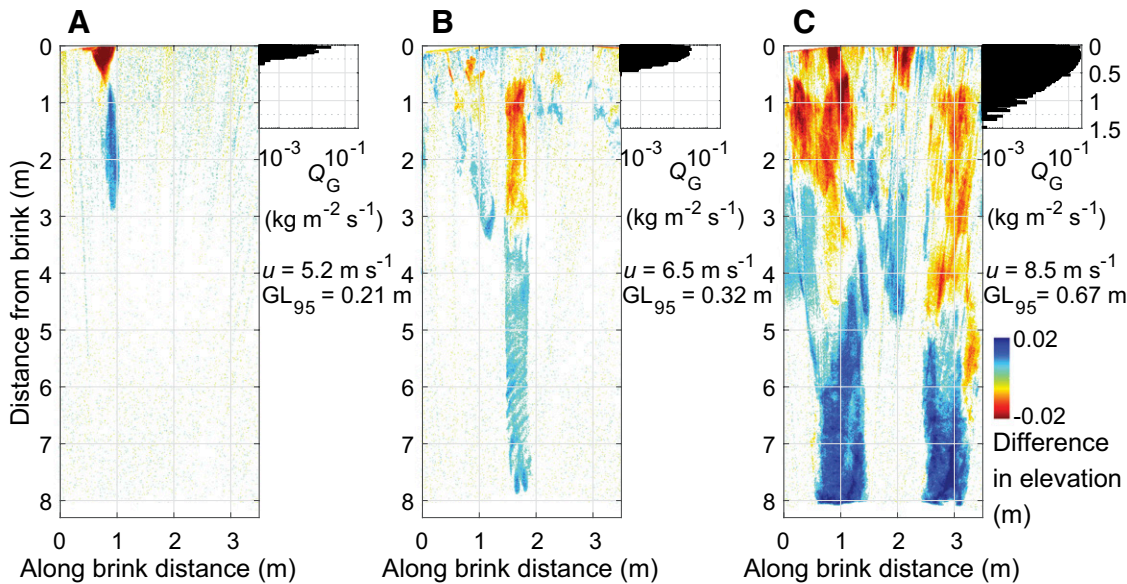
**Figure 3. A:** Mean deposition rate ( $\delta_D$ ) within the top 1 m of lee slope for the range of measured wind speeds. **B:** Variation in deposition flux with horizontal distance from the brink averaged for all runs within each of three different wind speed ( $u$ ) categories ( $<6$  m s<sup>-1</sup>,  $6$ – $8$  m s<sup>-1</sup>,  $>8$  m s<sup>-1</sup> where  $n = 27, 10,$  and  $14$ , respectively). Dashed line links position of peak  $\delta_D$  at different wind speeds.

Figure 5A. For winds  $<6$  m s<sup>-1</sup>, the dominant mode of failure frequency was at 0.3 m, while for  $>6$  m s<sup>-1</sup> the mode shifted further from the brink to 0.4 m, reaching 1 m for winds  $>8$  m s<sup>-1</sup>. The maximum distance at which failures were detected for the lower velocity winds was 1.1 m, but Figure 5A shows that for winds  $>8$  m s<sup>-1</sup>, avalanche initiation occurred as far as 6.4 m from the brink. Figure 5B examines the location of avalanche initiation related to values of  $GL_{95}$  and confirms that failure points are close to the brink for low grainfall lengths (e.g., all avalanches originate within 1.35 m of the brink for  $GL_{95} < 0.35$  m) and the wide spread in failure locations associated with greater values of  $GL_{95}$ .

The grainfall downwind of the brink and the subsequent downslope grainflow activity leads to advancement of the slip face (Fig. 6A) and downwind dune migration, but it is crucial that migration only occurs when the avalanches reach as far as the base of the slip face. The importance of grainfall characteristics in the upper 1 m of the slip face in this process is demonstrated by the fact that  $GL_{95}$  emerges as a better predictor of slip face topographic change ( $R^2$  0.9) than the saltation flux at the brink ( $Q_{sz}$ ;  $R^2$  0.85) (Fig. 6B).

## DISCUSSION

While there is some ambiguity in the literature, we find a clear relationship between  $\delta_D$  and wind speed (Figs. 3A and 3B). The resolution of the TLS allows us to offer the first field evidence identifying a peak in  $\delta_D$  near the brink (Fig. 3B), supporting the modeling output of Anderson (1988). It is significant that our data



**Figure 4.** Examples of typical change in surface elevation between sequential scans, illustrating avalanche behavior. **A:** Under conditions of low mean wind speeds. **B:** Under conditions of intermediate mean wind speeds. **C:** Under conditions of high mean wind speeds. Also shown with vertical scale is frequency histogram of derived grainfall flux distribution ( $Q_G$ ; log scale on x axis) for each case. See the GSA Data Repository<sup>1</sup> for animation of avalanches for each of the 51 scan periods.

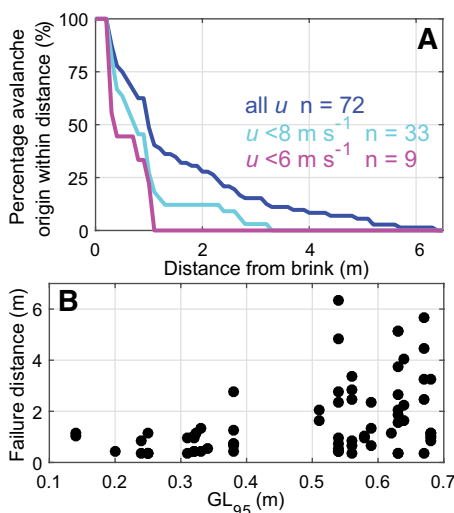


**Figure 5. A:** Cumulative frequency of detected point of avalanche origin with distance from the brink, including subsets of wind speeds ( $u$ ) below  $6 \text{ m s}^{-1}$  (magenta) and  $8 \text{ m s}^{-1}$  (cyan). **B:** Distance from brink of avalanche initiation (failure distance) as a function of maximum grainfall length ( $GL_{95}$ ).

also suggest a clear shift in the distance from the brink of this peak in  $\delta_D$  as wind speed increases (from 0.04 for winds  $< 6 \text{ m s}^{-1}$  to 0.06 m for winds  $> 8 \text{ m s}^{-1}$ ). This peak was not detected by Nickling et al. (2002) or Sutton et al. (2013b), possibly as a consequence of their leeside trap resolution and discretization.

A central issue of contention in linking grainfall to dune migration rate relates to the significance of wind speed as a driver of avalanche volume. Sutton et al. (2013a) reported no relationship between these variables in laboratory

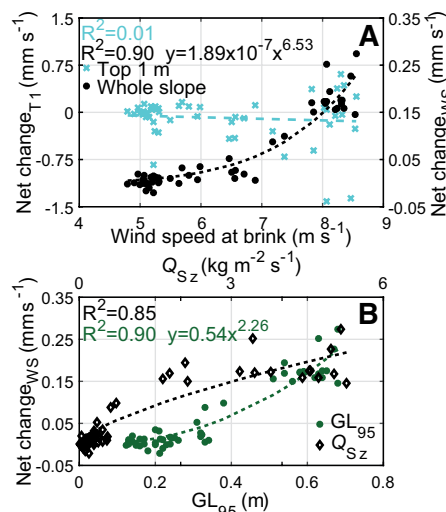


**Figure 6. A:** Rate of net surface height change (including grainfall and grainflow affected areas) for each scan period for both the top 1 m of the lee slope (T1) and the entire lee slope (WS), as a function of wind speed. **B:** Rate of net surface height change across the entire lee slope as a function of maximum grainfall length ( $GL_{95}$ , bottom x axis) and saltation flux at the brink (saltation flux,  $Q_{Sz}$ , top x axis).

experiments and suggested that avalanche frequency, rather than magnitude, increases with wind speed, supporting the results of McDonald and Anderson (1996) and Breton et al. (2008). While our data show a similar disconnect between wind speed and net surface change within the top 1 m of the lee slope (where surface change includes both grainfall and grainflow), we find that net surface change scales well with wind speed across the entire slip face

(power exponent 6.5;  $R^2$  0.9; Fig. 6A). It is notable, however, that the shape of the curve in Figure 6A illustrates negligible net surface change of the lee slope at low wind speeds ( $< 6 \text{ m s}^{-1}$ ).

While our data confirm an increase in avalanche frequency under stronger winds (Fig. 5), we also observed an increase in avalanche magnitude (both volume and extent; Fig. 4). Identifying drivers of avalanche magnitude is important because deposit thickness is crucial for interpreting dune stratigraphy (Anderson, 1988; McDonald and Anderson, 1996). The increase in avalanche magnitude with increasing wind speed in our study is indicated by the appearance of grainfalls that descend the entire lee slope, with deposition lobes that expand both in width (0.4 m to 1.13 m for  $u > 6 \text{ m s}^{-1}$ ) and depth (0.018 m to 0.03 m; e.g., Figs. 4B and 4C) when wind speeds exceed  $6 \text{ m s}^{-1}$ .

Our data therefore suggest that some caution should be exercised in using wind speed as a simple driver for dune migration rate. This is because at low wind speeds the value of  $GL_{95}$  is small and the location of  $Q_{Gm}$  is close to the brink (Figs. 2A and 3A). Low wind speeds trigger small avalanches that diminish within 1–2 m of travel (Fig. 4A), resulting in no net migration of the dune. In contrast, at high wind speeds the value of  $GL_{95}$  increases (maximum  $GL_{95} = 0.75 \text{ m}$ ) and the location of  $Q_{Gm}$  moves further downslope (Fig. 3B), resulting in a greater proportion of sediment being delivered further from the brink. This allows for the destabilization of a larger area of the lee slope because of the increased contribution to the avalanche from sediment destabilized above the point of failure (McDonald and Anderson, 1996; Sutton et al., 2013a). High wind speeds therefore

<sup>1</sup>GSA Data Repository item 2017071, additional methods and animations, is available online at [www.geosociety.org/datarepository/2017](http://www.geosociety.org/datarepository/2017), or on request from [editing@geosociety.org](mailto:editing@geosociety.org).



trigger proportionally larger avalanche failures (Fig. 4C) than low wind speeds. Furthermore, the existence of failures outside the grainfall zone (Fig. 5A) suggests that in high wind speeds secondary avalanches are also initiated further downslope in response to accumulation of sediment resulting from the primary avalanches on the upper slopes (e.g., McDonald and Anderson, 1996; Sutton et al., 2013a). Sediment delivery from these primary avalanches forms additional bulges of deposition as far as 6.4 m from the brink that eventually fail and move additional sediment to the slip face base.

At high wind speeds the dune migration rate is therefore intensified nonlinearly in comparison to lower wind speed conditions due to (1) higher values of brink saltation driven by the higher wind speeds, (2) larger avalanche failures caused by the downslope shift in peak grainfall flux, and (3) the triggering of secondary avalanche failures further down the slip face. The variability of the proportion of the slip face affected by grainfall is therefore a key control on avalanche dynamics and dune migration rate. Furthermore, the limited morphological impact on the dune lee slope caused by low wind conditions is likely to be obliterated by the large-scale morphological change induced in high wind conditions, the concept of sedimentary signal shredding (Jerolmack and Paola, 2010). The restriction of avalanches to the upper slopes of the slip face in low wind speed conditions, together with sedimentary signal shredding, implies that the aeolian signature of low-energy conditions in a dune environment is unlikely to be well represented in dune stratigraphy, and may be very difficult to resolve from the rock record (e.g., Eastwood et al., 2012). It also suggests that along with dune height (Kocurek and Dott, 1981), wind speed is an important driver of deposit stratigraphic thickness.

## CONCLUSIONS

In combining airflow and sand transport measurements with high-frequency TLS, this work offers a new approach for quantifying grainfall, one of the fundamental and most persistently poorly understood processes of deposition on aeolian dunes. For the first time, this field study identifies the process of grainfall zone expansion with increasing wind speed and recognizes its crucial role in intensifying avalanche dynamics on aeolian lee slopes. Our data indicate that a nonlinearity exists between wind speed and the magnitude of lee slope avalanching such that the imprint of low wind conditions on dune

migration dynamics is unlikely to be preserved in dune stratigraphy. Such low-energy conditions may therefore be underrepresented in interpretations of the rock record.

## ACKNOWLEDGMENTS

This study was funded by grants from the National Geographic Society Science and Exploration Europe (GEFNE110–14), the British Society for Geomorphology, and the NERC GEF (Natural Environment Council Geophysical Equipment Facility, 1025). Data processing used the IRIDIS High Performance Computing Facility at the University of Southampton. We thank the Namibia Ministry of Environment and Tourism, I. Matheus, J. Kazeurua, and Skeleton Coast National Park Rangers (permit 1913/2014), and J. Mayaud, M. David, S. Muinjo, B. Shiyanga, D. Beben, T. Bishop, and W. Nickling for field and instrument assistance. We also thank J. Schmitt, N. Lancaster, S. Sutton, and an anonymous reviewer for helping to improve this manuscript.

## REFERENCES CITED

- Anderson, R.S., 1988, The pattern of grainfall deposition in the lee of aeolian dunes: *Sedimentology*, v. 35, p. 175–188, doi:10.1111/j.1365-3091.1988.tb00943.x.
- Barchyn, T.E., Hugenholtz, C.H., Li, B., Neuman, C.M., and Sanderson, R.S., 2014, From particle counts to flux: Wind tunnel testing and calibration of the Wenglor aeolian sediment transport sensor: *Aeolian Research*, v. 15, p. 311–318, doi:10.1016/j.aeolia.2014.06.009.
- Breton, C., Lancaster, N., and Nickling, W.G., 2008, Magnitude and frequency of grain flows on a desert sand dune: *Geomorphology*, v. 95, p. 518–523, doi:10.1016/j.geomorph.2007.07.004.
- Eastwood, E.N., Kocurek, G., Mohrig, D., and Swanson, T., 2012, Methodology for reconstructing wind direction, wind speed and duration of wind events from aeolian cross-strata: *Journal of Geophysical Research*, v. 117, F03035, doi:10.1029/2012JF002368.
- Hesp, P.A., and Hastings, K., 1998, Width, height and slope relationships and aerodynamic maintenance of barchans: *Geomorphology*, v. 22, p. 193–204, doi:10.1016/S0169-555X(97)00070-6.
- Hodge, R., Brasington, J., and Richards, K., 2009, In situ characterization of grain-scale fluvial morphology using terrestrial laser scanning: *Earth Surface Processes and Landforms*, v. 34, p. 954–968, doi:10.1002/esp.1780.
- Hunter, R.E., 1977, Basic types of stratification in small eolian dunes: *Sedimentology*, v. 24, p. 361–387, doi:10.1111/j.1365-3091.1977.tb00128.x.
- Hunter, R.E., 1985, A kinematic model for the structure of lee-side deposits: *Sedimentology*, v. 32, p. 409–422, doi:10.1111/j.1365-3091.1985.tb00520.x.
- Jerolmack, D.J., and Paola, C., 2010, Shredding of environmental signals by sediment transport: *Geophysical Research Letters*, v. 37, L19401, doi:10.1029/2010GL044638.
- Kocurek, G., and Dott, R.H.J., 1981, Distinctions and uses of stratification types in the interpretation of eolian sand: *Journal of Sedimentary Petrology*, v. 51, p. 579–595, doi:10.1306/212F7CE3-2B24-11D7-8648000102C1865D.

- Kostaschuk, R., Shugar, D., Best, J., Parsons, D., Lane, S., Hardy, R., and Orfeo, O., 2009, Suspended sediment transport and deposition over a dune: Rio Parana, Argentina: *Earth Surface Processes and Landforms*, v. 34, p. 1605–1611, doi:10.1002/esp.1847.
- Lancaster, N., 1982, Dunes on the Skeleton Coast, Namibia (South West Africa)—Geomorphology and grain-size relationships: *Earth Surface Processes and Landforms*, v. 7, p. 575–587, doi:10.1002/esp.3290070606.
- McDonald, R.S., and Anderson, R.S., 1995, Experimental verification of aeolian saltation and lee side deposition models: *Sedimentology*, v. 42, p. 39–56, doi:10.1111/j.1365-3091.1995.tb01270.x.
- McDonald, R.R., and Anderson, R.S., 1996, Constraints on eolian grain flow dynamics through laboratory experiments on sand slopes: *Journal of Sedimentary Research*, v. 66, p. 642–653, doi:10.1306/D42683D3-2B26-11D7-8648000102C1865D.
- Nickling, W.G., Neuman, C.M., and Lancaster, N., 2002, Grainfall processes in the lee of transverse dunes, Silver Peak, Nevada: *Sedimentology*, v. 49, p. 191–209, doi:10.1046/j.1365-3091.2002.00443.x.
- Nield, J.M., and Wiggs, G.F.S., 2011, The application of terrestrial laser scanning to aeolian saltation cloud measurement and its response to changing surface moisture: *Earth Surface Processes and Landforms*, v. 36, p. 273–278, doi:10.1002/esp.2102.
- Nield, J.M., Wiggs, G.F.S., and Squirrell, R.S., 2011, Aeolian sand strip mobility and protodune development on a drying beach: Examining surface moisture and surface roughness patterns measured by terrestrial laser scanning: *Earth Surface Processes and Landforms*, v. 36, p. 513–522, doi:10.1002/esp.2071.
- Pelletier, J.D., Sherman, D.J., Ellis, J.T., Farrell, E.J., Jackson, N.L., Li, B., Nordstrom, K.F., Maia, L.P., and Omidyeganeh, M., 2015, Dynamics of sediment storage and release on aeolian dune slip faces: A field study in Jericoacoara, Brazil: *Journal of Geophysical Research*, v. 120, p. 1911–1934, doi:10.1002/2015JF003636.
- Silvestro, S., Fenton, L.K., Vaz, D.A., Bridges, N.T., and Ori, G.G., 2010, Ripple migration and dune activity on Mars: Evidence for dynamic wind processes: *Geophysical Research Letters*, v. 37, L20203, doi:10.1029/2010GL044743.
- Sutton, S.L.F., McKenna Neuman, C., and Nickling, W., 2013a, Avalanche grainflow on a simulated aeolian dune: *Journal of Geophysical Research*, v. 118, p. 1767–1776, doi:10.1002/jgrf.20130.
- Sutton, S.L.F., McKenna Neuman, C., and Nickling, W., 2013b, Lee slope sediment processes leading to avalanche initiation on an aeolian dune: *Journal of Geophysical Research*, v. 118, p. 1754–1766, doi:10.1002/jgrf.20131.

Manuscript received 11 August 2016

Revised manuscript received 30 November 2016

Manuscript accepted 1 December 2016

Printed in USA